

Small Crack Propagation in Multiaxial Notch Fatigue

K. Tanaka¹

¹ Department of Mechanical Engineering, Meijo University, Nagoya 468-8502, Japan
E-mail: ktanaka@meijo-u.ac.jp

ABSTRACT. *The present paper deals with torsional fatigue of circumferentially notched round bars of austenitic stainless steel and carbon steel without and with static tension. The torsional fatigue life of stainless steels was found to increase with increasing stress concentration under the same nominal shear stress amplitude. The electrical potential monitoring revealed that the crack initiation life decreased with increasing stress concentration, while the crack propagation life increased. The anomalous behavior of the notch-strengthening effect was ascribed to the larger retardation of fatigue crack propagation by crack surface contact. The superposition of static tension on cyclic torsion causes notch weakening. The notch-strengthening effect in torsional fatigue was not found in carbon steels. The difference in the crack path of small cracks near notch root between stainless steel and carbon steel gives rise to the difference in the notch effect in torsional fatigue.*

INTRODUCTION

Fatigue fracture of several engineering components such as transmission shafts, pipes and springs occurs under combined torsional and axial loading. Notches or stress concentrations are the common site of crack initiation. The assessment of the notch effect on the fatigue strength and life is essential in fatigue designs. In comparison with axial fatigue, torsional fatigue studies have been relatively limited, and the combination of torsional and axial loading further complicates the assessment of the fatigue strength and life. Since fatigue fracture results from the initiation and propagation of fatigue cracks, the understanding of small crack behavior greatly helps to improve the accuracy of the fatigue life prediction of notched components.

An anomalous phenomenon of the notch-strengthening effect was found in torsional fatigue of circumferentially notched round bars of austenitic stainless steels [1,2]. The fatigue life of notched bars was found to be longer than that of smooth bars, and to increase with increasing stress concentration under the same amplitude of the nominal shear stress. The anomalous notch-strengthening was not found in carbon steels [3]. In the present paper, the propagation behavior of small cracks was observed by the scanning electron microscopy (SEM) and continuously monitored by the electrical potential method. The difference in the notch effect between stainless steel and carbon steel is discussed on the basis of the crack path morphology of small cracks near the notch root observed by SEM.

EXPERIMENTAL PROCEDURE

The material used is hot rolling austenitic stainless steel (JIS SUS316L) and carbon steel (JIS SGV410) for nuclear power plant [1,3]. The specimen was machined from solution-treated hot-rolled bars in the direction whose longer direction coincides with the rolling direction. The diameter of the gage section of smooth specimens is 16mm (named SM-M specimen) or 10.5mm (SM specimen), and the length is 40 mm. Figure 1 shows the shapes of notched specimens which have circumferential notches with three different root radii. The specimens with the radii 4.5, 1.07, and 0.22mm are named NA, NB, and NC specimens. All the specimens were finished by buffing using diamond past. The elastic stress concentration factor for the shear stress under torsion for NA, NB, and NC specimens was calculated by the finite element method as 1.17, 1.55, and 2.54, respectively. Moreover, specimens which have 1.5 times larger dimensions of NA specimens, named NA-M specimens, are used for microscopic observation near the notch root.

Fatigue tests were performed with a tension-torsion biaxial electro-servo-hydraulic testing machine. Fatigue testing was done under load-controlled conditions with the load ratio R of -1. The waveform of the cyclic load was triangular and the frequency was between 0.2 and 2.0Hz. The fatigue test under cyclic torsion without static tension is called case A and that with static tension case B. The applied shear stress amplitude was expressed in terms of the nominal stress calculated elastically from the applied torque for the minimum cross section, and the static tensile stress applied in case B is the same as the applied amplitude of the shear stress. The direct-current electrical potential method was used for monitoring crack initiation and propagation.

Fatigue fracture surfaces were observed by SEM. The 3-D topography was constructed from stereo-pair pictures by using a commercial software, Mex 5.1.

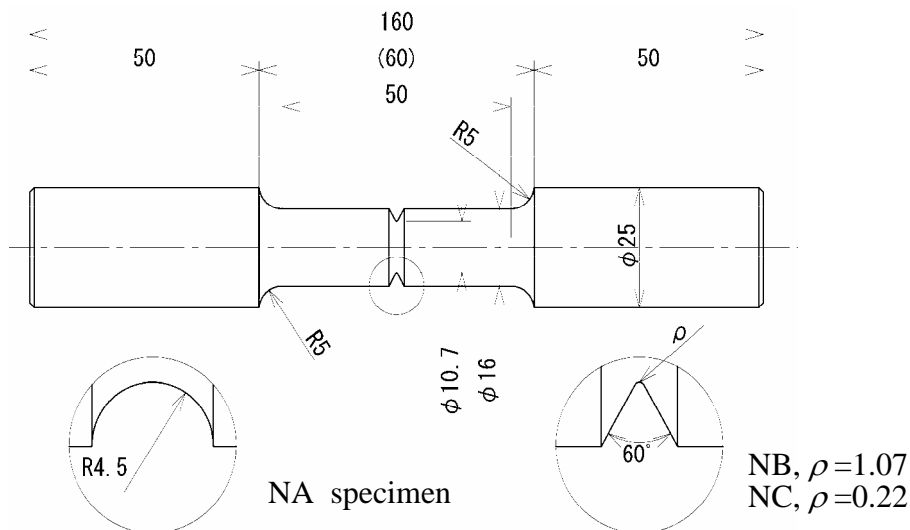


Figure 1 Shape and dimensions of notched specimens (dimensions are in mm).

EXPERIMENTAL RESULTS AND DISCUSSION

S-N Curves

The relations between the shear stress amplitude and the number of cycles to failure in case A are shown in Fig. 2, where (a) is for SUS and (b) is for SGV. It should be noted that the fatigue life of notched specimens of SUS becomes longer, as the notch gets sharper and stress concentration factor larger. This anomalous notch-strengthening is more evident for lower stress cases of 180 and 160 MPa. When a static tension was superposed as in case B, notch-strengthening effect for SUS disappeared and ordinary notch-weakening was observed as reported in our previous paper [2]. The fatigue life of SGV gets shorter for sharper notches in case A and also in case B.

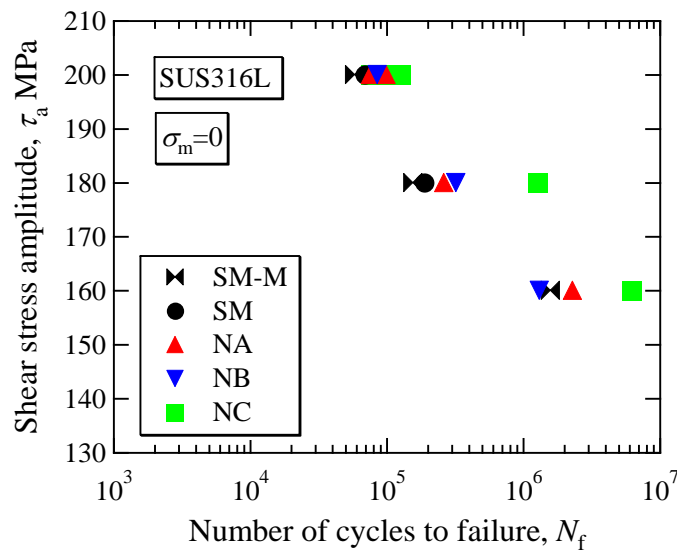


Figure 2(a) *S-N* relation for SUS316L.

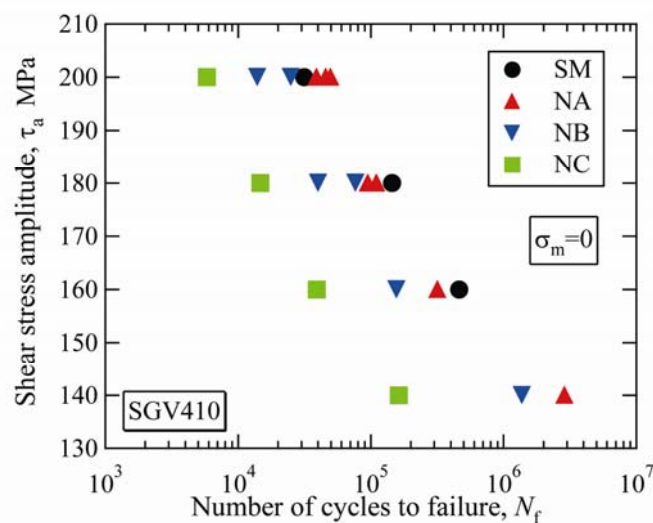


Figure 2(b) *S-N* relation for SGV410.

Change of Electrical Potential during Fatigue

The change in the electrical potential under cyclic shear stress amplitude of 180MPa in case A for SUS is shown in Fig. 3(a), where the electrical potential was normalized by the initial value. The number of stress cycles at point where the electrical potential shows a rapid increase is considered to indicate crack initiation. It is interesting to note that NC specimen shows the earliest rise in the electrical potential, followed by NB specimen and NA specimen. The crack initiation life is shorter as the notch gets sharper.

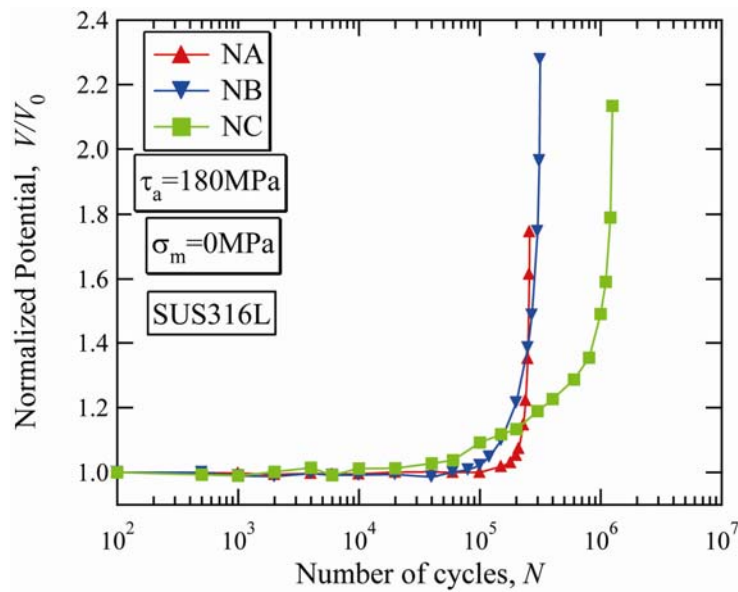


Figure 3(a) Change of electrical potential during fatigue of SUS316L in case A.

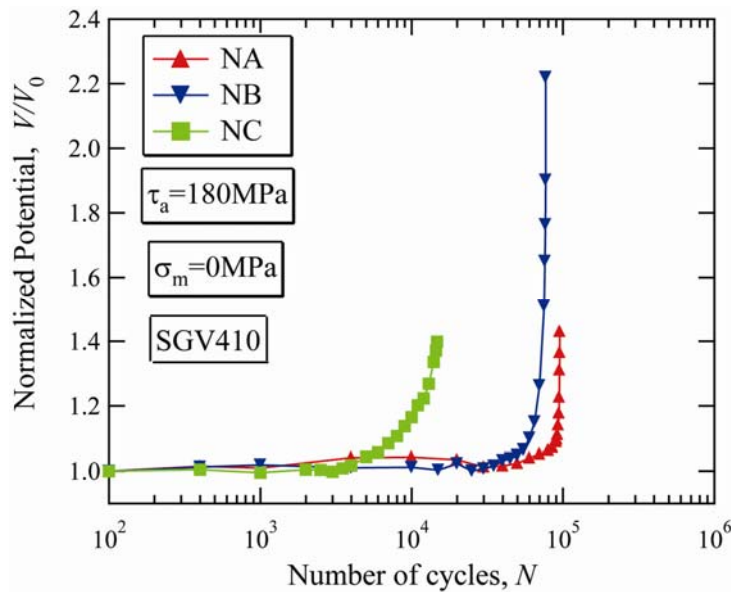


Figure 3(b) Change of electrical potential during fatigue of SGV410 in case A.

However, the rising speed of the electrical potential is slowest for NC specimen. The potential of NB and NA specimens catches up the potential of NC specimen. The final fatigue life is longer in the order of NA, NB, and NC specimens. In conclusion, the crack initiation life is shorter while the crack propagation life longer as the notch becomes sharper. Similar results were obtained for the case of the stress amplitudes of 160 and 200MPa. When a static tension is superposed on cyclic torsion, in case B, both crack initiation and propagation lives were shorter as sharper notches [2].

Figure 3(b) shows the change of the electrical potential during fatigue under 180MPa in case A for SGV. The rising point of the electrical potential and the final fracture are shorter for sharper notches.

Crack Initiation Life and Notch-Root Cyclic Strain

Figure 4(a) and (b) shows the relation between the stress amplitude and the number of cycles to crack initiation in case A of SUS and SGV determined by the rising point of the electrical potential. For all stress amplitudes, the crack initiation life is shorter for sharper notched specimens. When compared at the same shear amplitude, the crack initiation life of SUS is longer than that of SGV. The smaller strain amplitude at the notch root of SUS results in the longer crack initiation life in comparison with SGV.

The finite element method (FEM) analysis of elastic-plastic stress-strain was conducted for three types of notched specimens using cyclic stress-strain relation obtained by using hollow cylinders [4]. The equivalent strain amplitude is larger for sharper notches under the same nominal shear stress amplitude. It was concluded in our previous paper [4] that the crack initiation life of SUS was nearly controlled by the maximum value of the strain amplitude, and more precisely by the strain amplitude at a certain structural distance of 0.1 mm from the notch root in the strain distribution

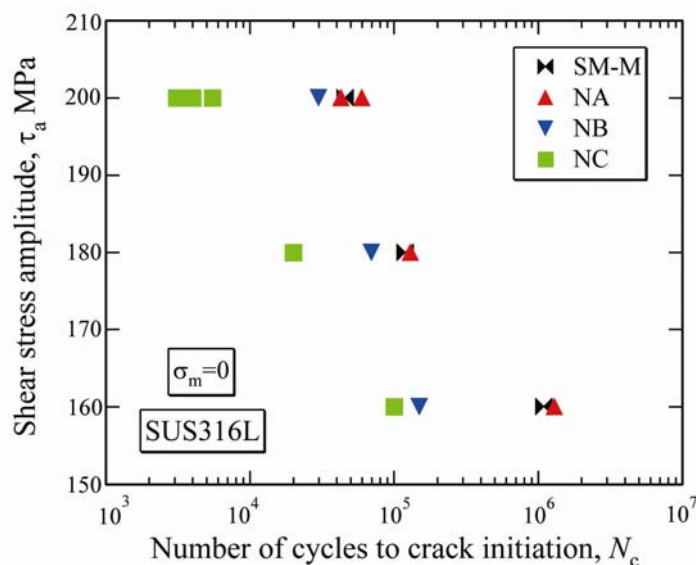


Figure 4(a) Relation between stress amplitude and the number of cycles to crack initiation for SUS316L in case A.

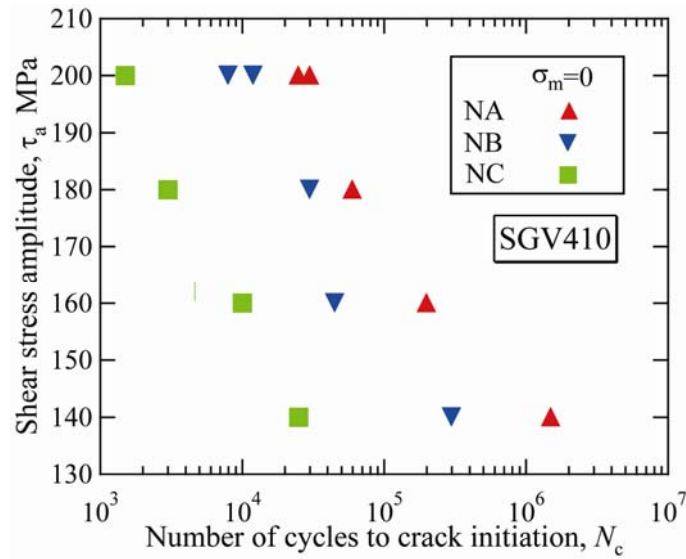


Figure 4(b) Relation between stress amplitude and the number of cycles to crack initiation for SGV410 in case A.

calculated by the elastic-plastic FEM. All the crack initiation life for notched specimens with different root radii merged to the strain-life relation of smooth hollow cylinders.

A similar analysis was conducted for the case of SGV. When compared at the same stress amplitude, the strain amplitude at the notch root of SGV was larger than that of SUS, because SGV was softer than SUS. The crack initiation life of SGV was nearly controlled by the strain amplitude at the notch root, and more precisely about 0.1mm distant from the notch root. The relation between the equivalent strain amplitude and the crack initiation life is not much different between SUS and SGV.

Crack Propagation Behaviour

Figure 5 shows optical micrographs taken at the notch root of notched NA-M specimens of SUS whose fatigue test was stopped at the normalized electrical potential of $V/V_0=1.10$ in cases A and B. The longitudinal direction (loading-axis) of the specimen is vertical. Stage I cracks nucleated vertically or horizontally along the maximum shear planes are branched to 45 degree, showing tensile Stage II propagation. In case A, cross-shaped tensile cracks extend out of the notch region where the stress is low. The connection of cross-shaped cracks results in zigzag fracture path, producing factory-roof appearance on the fracture surface. The sliding contact of the zigzag shaped fracture surface gives rise to the retardation of crack propagation [6]. When the static tension is superposed on cyclic torsion as in case B, cross-shaped cracks branching from Stage I cracks are connected vertically, perpendicular to the tensile direction. The degree of tortuosity is lower in case B than in case A, suggesting less amount of retardation of crack propagation. The superposition of static tension opens cracks and promotes the vertical extension of shear cracks of Stage I [7].

Figure 6 shows cracks formed at the notch root of NA-M specimens of SGV whose fatigue tests were stopped at the normalized electrical potential of $V/V_0=1.05$ in cases A

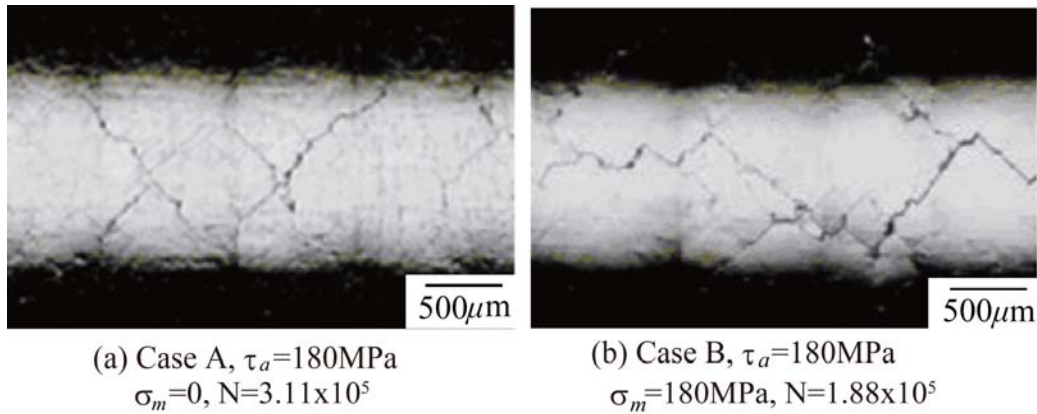


Figure 5 Optical micrographs of NA-M specimens of SUS316L fatigued under $\tau_a=180\text{MPa}$ at $V/V_0=1.10$.

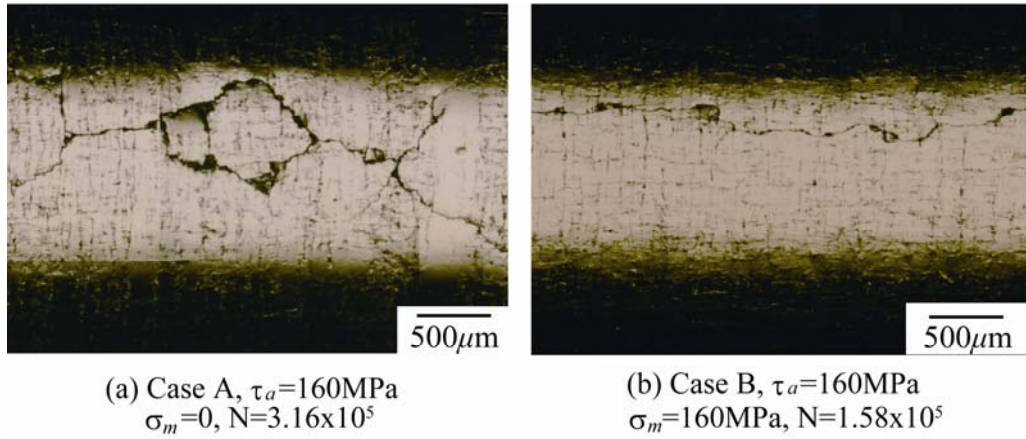


Figure 6 Optical micrographs of NA-M specimens of SGV410 fatigued under $\tau_a=160\text{MPa}$ at $V/V_0=1.05$.

and B. The crack propagates nearly horizontally for case B. Even in case A, the 45 degree propagation of cracks is less evident and the connection of cracks takes place along the horizontal direction at the notch root.

The propagation behaviour of cracks was evaluated from the change of electrical potential. The crack is assumed to propagate from the root of circumferential notch toward the centre of the bar concentrically. This assumption may be justified, because the electrical potential corresponds to the projection of the crack area on the minimum cross section. The relation between the crack length and the electrical potential was determined by the FEM analysis of the direct current electric field [5]. Using this relation, the crack length was estimated from the potential, and the crack propagation rate was calculated by the secant method.

Figure 7(a) shows the change of the crack propagation rate with crack length for NA, and NC specimens of SUS under the shear stress amplitude of 180 MPa in case A

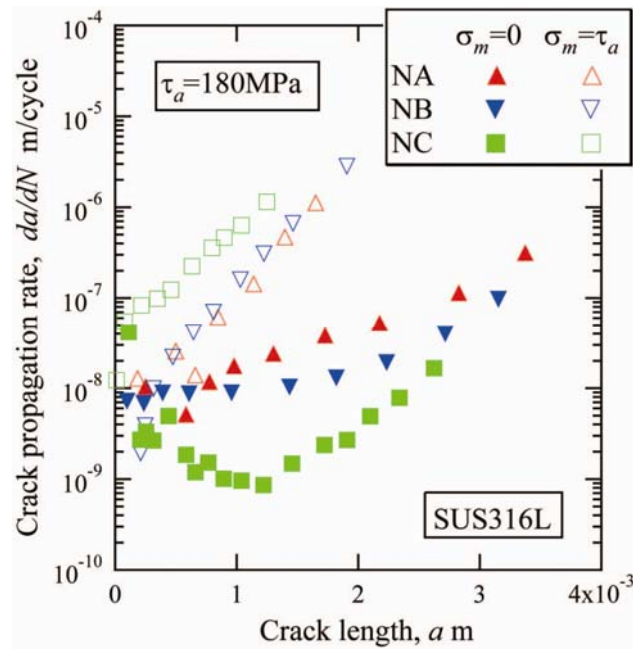


Figure 7(a) Change of crack propagation rate with crack length in SUS316L under cyclic torsion $\tau_a=180\text{MPa}$ in cases A and B.

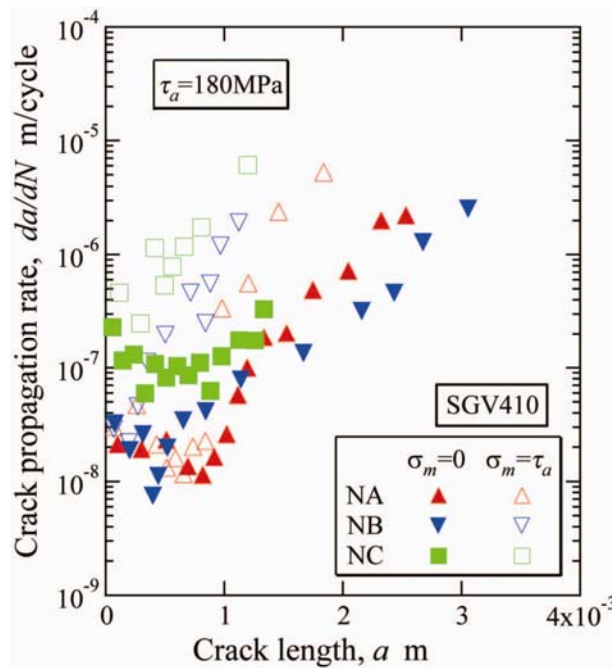


Figure 7(b) Change of crack propagation rate with crack length in SGV410 under cyclic torsion $\tau_a=180\text{MPa}$ in cases A and B.

and B. In case A, the crack propagation rate decreases or nearly remains constant at short crack length and then turn to increase after taking the minimum growth rate at the crack length of 1mm. When compared at the same crack length, the crack propagation rate is lower for sharper notches, and the amount of retardation is larger. In case B, the crack propagation rate increases with increasing crack length. When compared at the same crack length, the crack propagation rate is higher for sharper notches, corresponding to the higher stress intensity factor [5].

Figure 7(b) shows the results for SGV. In case A, the crack propagation rate shows a similar change with the crack length as for SUS. When compared at the same crack length, the propagation rate is higher for sharper notches, contrary to the case of SUS. In case B, the change of the crack propagation rate is similar to the case of SUS.

When the shear stress is high and a static tension is superposed, the crack shows shear mode crack propagation, and the crack propagation life can be predicted using the *J*-integral range [2,8].

Fractography

After the fatigue tests, the specimens were broken by tension. Examples of SEM micrographs of fracture surfaces of notched SUS specimens in case A are shown in Fig. 8, where the white line indicates the locus used for 3-D topographic measurement as described later. The factory-roof shape is observed in all fracture surfaces. The characteristics of the factory roof can be explained based on the crack path illustrated in Fig. 9. Small shear cracks of Stage I formed at the notch root turn to cross-shaped cracks showing tensile Stage II mode propagation. They are confined by the notch region, because of the difficulty getting out of the notch mouth. The connection of cross-shaped cracks results in the factory roof on fracture surfaces. The shape of the factory roof becomes finer with increasing stress level as seen from the comparison among Figs. 8(a), (b) and (c), or between (e) and (f). More crack nucleation sites operates as the stress amplitude increases, resulting in finer size of factory roof. At a high stress of 200MPa, the edge of the triangular shaped roof is rounded by rubbing between fracture surfaces as seen in Figs. 8(a) and (e). The factory-roof shape also becomes finer as the notch gets sharper as seen from the comparison among Figs. 8(b), (d) and (f), or between (a) and (c). More number of crack nucleation sites may operate at the root of sharper notches because the strain amplitude is larger for sharper notches, and also the narrow width of notches inhibits the propagation of cross-shaped Stage II cracks. On the other hand, for blunt notches, the strain amplitude is low and 45 degree propagation extends longer, resulting in less number of roof mountains. For very sharp notches, the initial flat fracture surface turns to factory-roof type as the crack extends as shown in Fig. 8(f) [6].

Striations can be seen on the factory-roof fracture surface as shown in Fig. 10, where NA specimen was fatigued under $\tau_a=180\text{MPa}$ in cases A. Figure (b) is the blow-up of the square area in Fig. (a), Fig. (c) is that of (b), and Fig. (d) is that of (c). In Fig. (d) striations are clearly seen on the fracture surface, showing Stage II tensile propagation. It is interesting to note that striations indicate the circumferential direction of crack propagation, that is the downhill direction of the factory roof, but not toward the center of the bar.

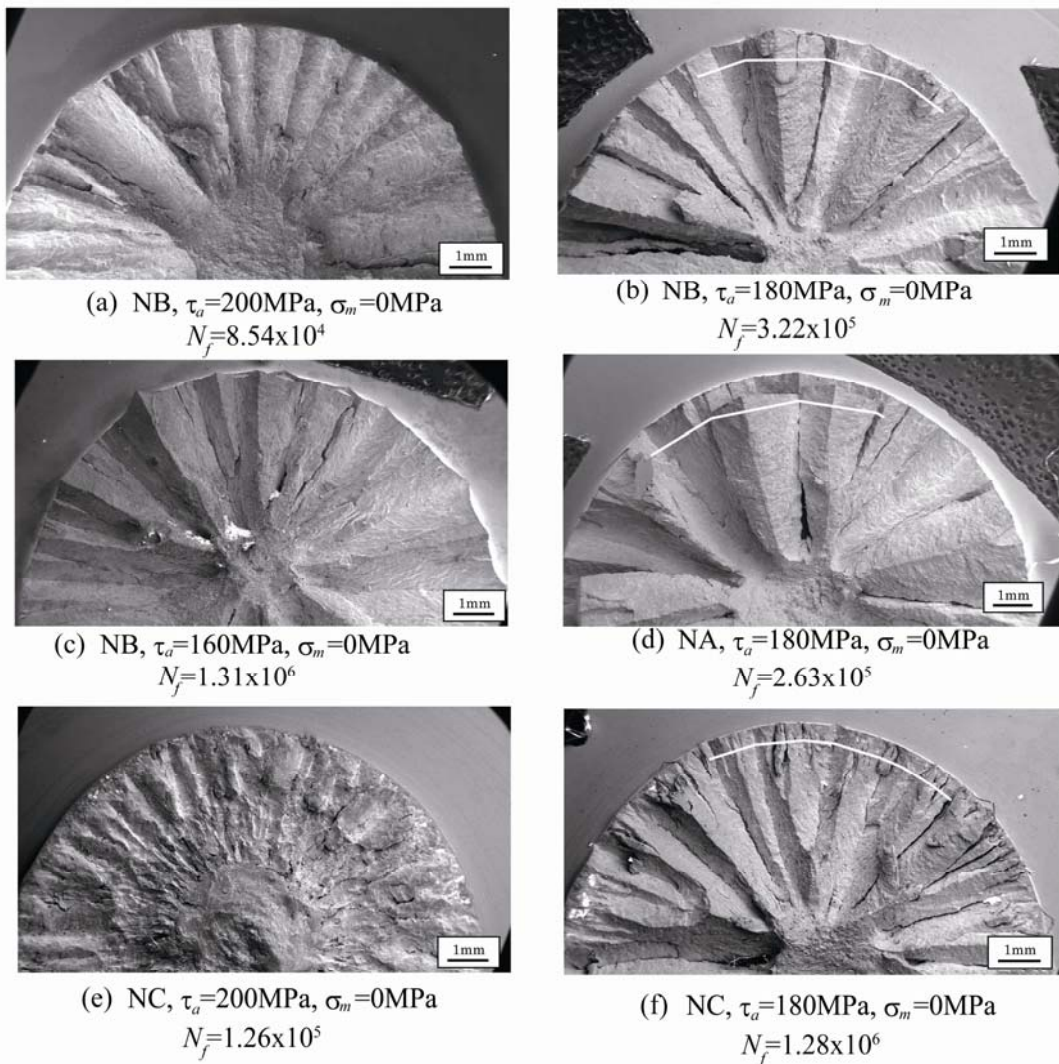


Figure 8 Fracture surfaces of SUS316L in case A.

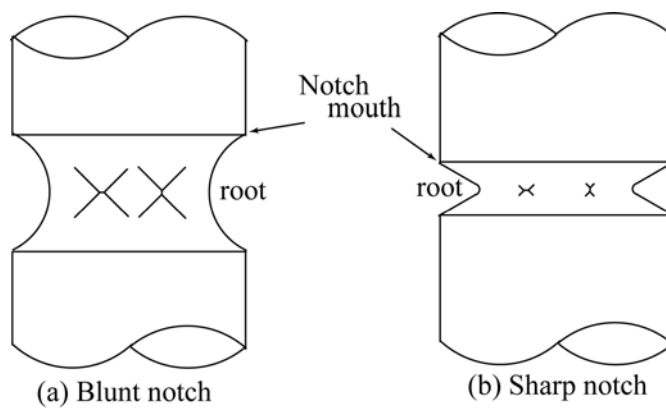


Figure 9 Cross-shaped cracks at the notch root.

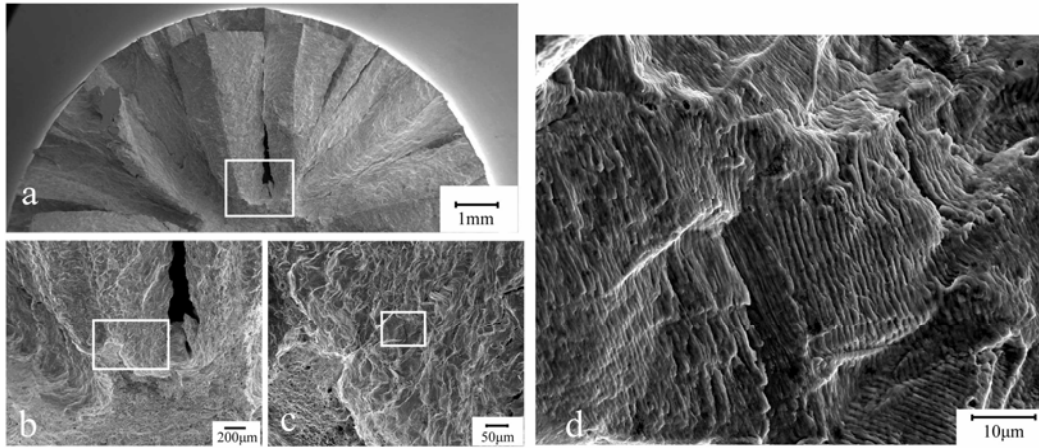


Fig. 10 Striation formed on factory-roof, NA, $\tau_a=180\text{MPa}$, $\sigma_m=0\text{MPa}$.

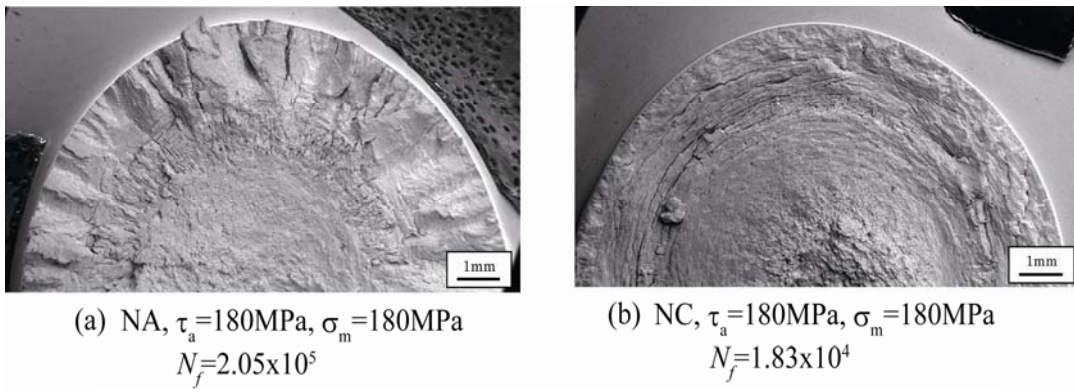


Figure 11 Fracture surfaces of SUS316L in case B.

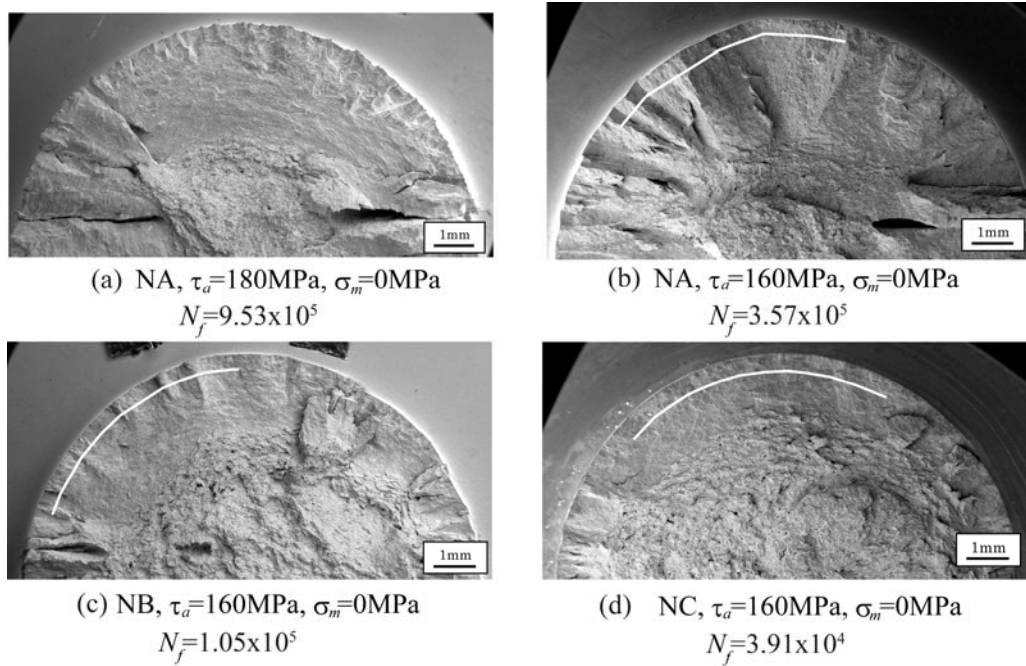


Figure 12 Fatigue fracture surface of SGV410 in case A.

In case B, the factory roof becomes less evident. Figure 11 shows examples of SEM micrographs of notched specimens fatigued under the stress amplitude of 180MPa in case B. The fracture surface of NC specimen fatigued at high stresses is smeared and the crack propagation takes place by mode III sliding as seen in Fig. 11(b), while at lower stresses for NA specimen, the factory roof exists at some part of the fracture surface as seen in Fig. 11(a). Whether the crack propagates in mode III fashion may be controlled by the amplitude of the shear displacement ahead of the crack tip.

Examples of fracture surfaces of SGV in case A are shown in Fig. 12. The flatness of the fracture surface increases as the stress amplitude is higher and the notch gets sharper. The formation of the factory roof is visible at low stresses and blunter notches as seen in Fig. 12(b). The stress level for the formation of shear mode flat fracture surface is higher for SUS than for SGV. For SUS, the factory roof is evident even at 200MPa, while the stress amplitude of 160 MPa is not low enough to form the factory roof on the fracture surface. At the stress amplitude of 140MPa, the factory roof fracture surface was observed on the fatigue fracture surface [3]. Since the strain amplitude at the notch root of SGV at 160MPa is roughly equal to that under 180MPa for SUS, SGV is more prone to shear mode crack propagation than SUS.

Three-Dimensional Topography of Fracture Surface

The three dimensional topography of fracture surfaces were constructed by using stereo pair of SEM micrographs using a commercial software, Mex 5.1. The topographic profile of the fracture surface is obtained along the periphery at about 0.5 mm from the surface. The locus is shown with the white line in Figs. 8 and 10. Following discussion will be focused on the profile in case A where the crack retardation is large.

The profiles of SUS taken from different notches under the stress amplitude of 180MPa are shown in Fig. 13. The slope angle of mountain-chain profiles is about 45 degree, showing the tensile mode crack propagation. The triangular shape of mountains are evident for all case. The size of one mountain is larger for blunter

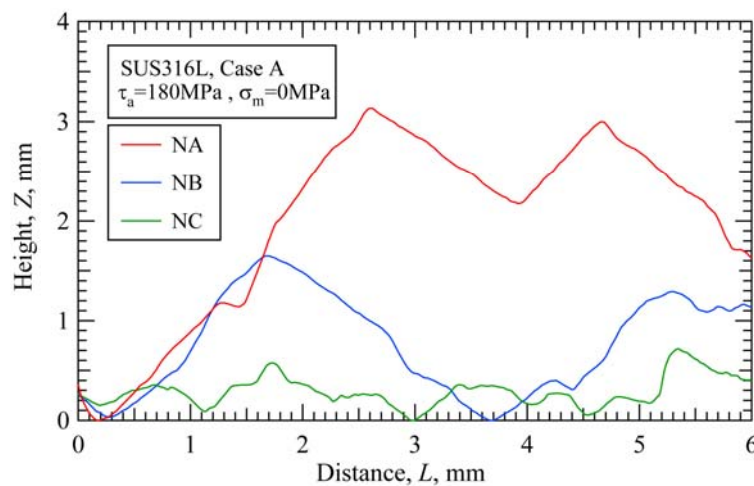


Figure 13 Topography of fatigue fracture surface of SUS316L for case A. (Effect of notch geometry).

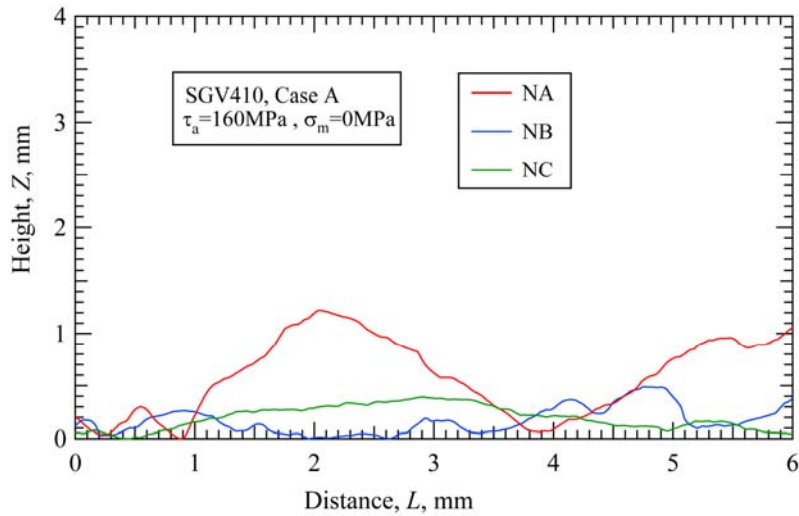


Figure 14 Topography of fatigue fracture surface of SGV10 for case A.
(Effect of notch geometry)

notches. With the reference to the crack propagation behaviour shown in Fig. 7, the crack retardation is larger for sharper notches, while the mountain size becomes smaller. Larger amount of retardation for sharper notches is related to the width of the notch region (see Fig. 9). The propagation cross-shaped tensile cracks will be blocked by the notch mouth because of less concentration of stress. The notch region is smaller for sharper notches, and cracks will be blocked at smaller crack lengths, resulting in a larger amount of retardation.

The profiles for SGV taken from different notches under the low stress amplitude of 160 MPa are shown in Fig. 14. The roughness is largest for bluntly notched NA specimens, corresponding to the largest amount of retardation for NA specimens as seen in Fig. 7(b). The crack retardation is reduced for sharper notches, because the fracture surface becomes smoother.

Fatigue Crack Path in Torsional Fatigue

The fatigue process of torsional fatigue of circumferentially notched bars is as follows: Stage I cracks are first formed along the maximum shear plane and propagate in shear mode for a short distance. Then, Stage II cracks branched to 45 degree with respect to the loading axis, showing tensile mode propagation. Stage II cracks extend out of the notch region where the stress is low, and then decelerate. The connection of 45 degree cracks results in zigzag crack path, producing factory-roof appearance on the fracture surface. The connection of shear cracks at high stresses results in shear mode fracture with the flat fracture surface.

Table 1 summarizes the factor controlling the transition from tensile to shear mode. For a given notch shape under the same stress amplitude, SGV is softer than SUS and the strain amplitude at the notch root is higher, which tends to show shear crack propagation. Furthermore, in contrast to a planar slip character of SUS, the slip deformation of SGV is wavy and easy to cross slip. The direction of crack propagation

Table 1 Tensile versus shear crack propagation.

Crack path	Tensile mode \longleftrightarrow Shear mode	
Material	SUS	SGV
Notch shape	Blunt	Sharp
Applied stress	Low stress	High stress Superposed static tension

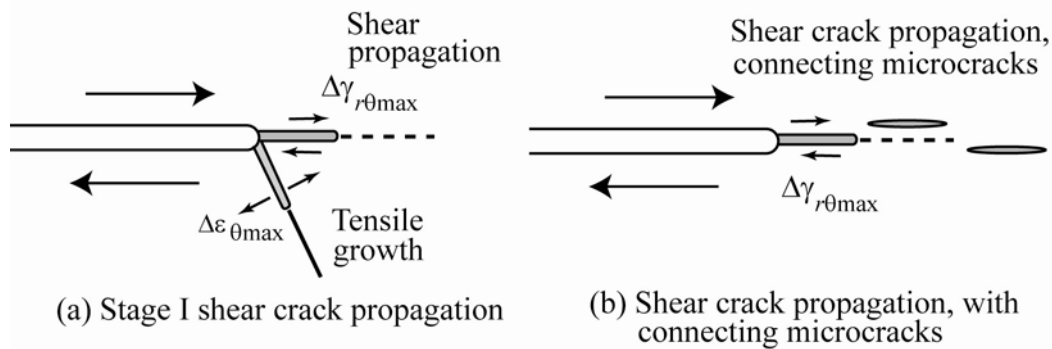


Figure 15 Shear crack propagation.

is prone to change, giving rise to ill-defined factory-roof shape of fracture surfaces. Further, a high work-hardening character of SUS may remain the factory-roof shape from smearing by rubbing. Murakami and others [9] proposed the condition of the transition from shear mode (Stage I) to tensile mode (Stage II) based on the shape change of semielliptical surface cracks. Frictional stress acting on the shear crack plane is also an important factor for the transition [10], and also the value of shear strain range ahead of the crack tip may be a candidate criterion as shown in Fig. 15. Stage I cracks nucleated along slip planes initially extend in shear mode, and the development of friction caused by the crack face contact reduces the true crack-tip shear strain range, resulting in the transition to branched cracks in tensile mode. High applied stresses nucleate abundant shear cracks ahead of the main crack and the connection of shear cracks promotes shear fracture. Superposition of static tension perpendicular to shear cracks reduces the friction of crack faces, again extension of shear crack propagation. Sharper notches usually have higher strain at the notch root and more abundant crack nucleation, again promoting shear fracture.

CONCLUDING REMARKS

In torsional fatigue of circumferentially notched bars of austenitic stainless steel, the fatigue life of notched bars was found to be longer than that of smooth bars and to increase with increasing stress concentration under the same amplitude of the nominal shear stress. This notch-strengthening effect is anomalous for the conventional fatigue design criterion. The electrical potential monitoring of the initiation and propagation of small cracks at the notch root showed that the crack initiation life decreased with increasing stress concentration, while the crack propagation life increased. The anomalous behavior of the notch-strengthening effect was ascribed to the larger retardation of fatigue crack propagation by crack surface contact for the sharper notches. The superposition of static tension reduced the retardation due to the smaller amount of crack surface contact, which gave rise well-known notch-weakening of the fatigue strength. This notch-strengthening effect was not found in torsional fatigue of carbon steel. The difference in the crack path of small cracks near notch root between stainless steel and carbon steel results in the difference in the notch effect in torsional fatigue.

The total fatigue life is the sum of crack initiation life and propagation life. The crack initiation life is controlled by the strain distribution near the notch root, and predictable from the fatigue life of the smooth hollow cylinders on the basis of FEM elastic plastic analysis. The crack propagation life can be predicted using an elastic-plastic fracture-mechanics parameter, such as the J -integral range, when the static tension is superposed on cyclic torsion. Under cyclic torsion without static tension, the shielding by crack face sliding contact greatly reduces the crack propagation rate, which should be quantified to predict the crack propagation life in the future.

REFERENCES

1. Tanaka, K., Hashimoto, A., Narita, J., Egami, N. (2009) *J. Soci. Mater. Sci., Japan*, **58**, 1044-1050.
2. Tanaka, K. (2010) *Procedia Eng.*, **2**, 27-36.
3. Tanaka, K., Ishikawa, T., Narita, J., Egami, N. (2011) *J. Soci. Mater. Sci., Japan*, **60**, 783-789.
4. Tanaka, K., Hiraiwa, T., Kozawa, M., Kimachi, H. (2011) *Trans. Japan Soci. Mech. Eng.*, **A77**, 335-344.
5. Tanaka, K., Ishikawa, T., Sakagawa, Y., Narita, J., Hiraiwa, T., Egami, N., (2011) *Trans. Japan Soci. Mech. Eng.*, **A77**, 402-414.
6. Tschegg, E. K. (1983) *J. Mater. Sci.*, **18**, 1604-1614.
7. Otsuka, A., Mori, K., Oshima, T., Tsuyama, S. (1980) *J. Soci. Mater. Sci., Japan*, **29**, 1042-1048.
8. Tanaka, K., Akiniwa, Y., Nakamura, H. (1986) *Fatigue & Fract. Eng. Mater. Struct.*, **19**, 571-579.
9. Murakami, Y., Takahashi, K., Toyama, K. (2005) *Fatigue & Fract. Eng. Mater. Struct.*, **28**, 49-60.
10. Doquet, V., Frelat, J. (2001) *Fatigue & Fract. Eng. Mater. Struct.*, **24**, 207-214.